Research Square

Preprints are preliminary reports that have not undergone peer review.
They should not be considered conclusive, used to inform clinical practice,
or referenced by the media as validated information.

Biomechanical Study of a Novel External Fixation Frame Controlling Postoperative Loss of Reduction in Thoracolumbar Fractures: Finite Element Analysis

Hui Guo
Chinese PLA General Hospital
Jiahao Feng
Chinese PLA General Hospital
Yanyan Xue
Aerospace Center Hospital
Kun Wang
Chinese PLA General Hospital
Ming Hao
Chinese PLA General Hospital
Shaobo Nie
nieshaobo301@163.com
Chinese PLA General Hospital

Research Article

Keywords: Minimally invasive, Spinal external fixation, Finite element analysis, Biomechanics, Thoracolumbar burst fractures, Micro-motion

Posted Date: July 5th, 2026

DOI: https://doi.org/10.21203/rs.3.rs-9891373/v1

License: This work is licensed under a Creative Commons Attribution 4.0 International License.
Read Full License

Additional Declarations: No competing interests reported.

Abstract

Objective

This study aims to investigate the biomechanical characteristics of percutaneous pedicle screw fixation combined with a novel external fixation device (Micro-Adjustable External Fixation - MAEF) for minimally invasive spinal fracture treatment using finite element analysis, providing theoretical support for clinical application.

Methods

We simulated an L1 vertebral fracture and constructed two finite element models: CASE 2: Percutaneous Short-Segment Intermediate Screw Fixation (PSISF)). Under load control, we recorded the percentage change in ROM values before and after fixation for both models, along with maximum stress values at the fixation system, fractured vertebra (L1), T12 inferior endplate, and L2 superior endplate.

Results

Under all loading conditions, the ROM of the MAEF model ranged from 8.4% to 15.5% of the normal lumbar spine model (T11-L3), while the PSISF model exhibited ROM values between 48.0% and 70.9% of the normal lumbar spine model (T12-L2). Compared with the PSISF model, the MAEF model exhibited lower maximum stress values in the fixation system, fractured vertebra (L1), inferior endplate of T12, and superior endplate of L2. Furthermore, the maximum stress values for the fixation systems in both models occurred under lateral rotation conditions: the MAEF model's fixation system peaked at 77.025 MPa during right rotation, while the PSISF model's fixation system peaked at 170.97 MPa during left rotation. Significantly, contrary to the PSISF model results, the fractured vertebral body (L1) in the MAEF model exhibited markedly higher maximum stress values during flexion and extension compared to lateral flexion, lateral extension, left rotation, and right rotation. These values were comparable to the maximum stresses observed in the PSISF model during flexion and extension, a phenomenon attributed to the MAEF model's micro-adjustable system. Additionally, under all loading conditions, the maximum stress values at the adjacent vertebral endplates in the MAEF model were lower than those in the PSISF model.

Conclusion

Compared to PSISF, MAEF exhibits superior stress distribution and provides enhanced stability. Its micro-adjustable system permits mechanical stimulation of fractured vertebrae during flexion/extension, preventing stress shielding. Theoretically, MAEF may reduce postoperative fixation system failure and kyphosis occurrence while accelerating fracture healing.

1. Introduction

Thoracolumbar burst fractures are the most common type of spinal fracture, frequently resulting from traffic accidents and falls from height[1-3] . The optimal surgical approach for traumatic thoracolumbar burst fractures (TTBFs) without neurological injury remains controversial. Current research increasingly favors percutaneous short-segment interbody screw fixation (PSISF)[4, 5] . Percutaneous minimally invasive treatment offers low trauma, and placing screws within the fracture segment enhances short-segment fixation stability. However, PSISF still has biomechanical limitations such as stress concentration and insufficient anterior support, potentially leading to complications like internal fixation failure and progressive kyphotic deformity[6, 7] . To address insufficient anterior support, some researchers have employed techniques like vertebral augmentation or combined anterior-posterior approaches to enhance anterior support strength[8-11]. While these methods reduce the incidence of internal fixation failure, they still cannot prevent worsening kyphosis after internal fixation removal[12, 13] .

Our department has designed a novel micro-adjustable external fixation system (MAEF) that offers a potential solution to this problem. Four pedicle screws on each side of the injured vertebra enhance fixation and reduction strength. The reinforced external frame provides superior fixation strength, and the modular, adjustable design of this structure allows for further fine-tuning to address potential loss of reduction. Furthermore, localized micro-motion following callus formation at the fracture site can stimulate callus development and prevent progressive kyphotic deformity. Our previous research has demonstrated the efficacy of MAEF in the treatment and maintenance of reduced thoracolumbar fractures[14], particularly as a viable option for patients with TTBFs undergoing percutaneous minimally invasive procedures. However, the potential biomechanical properties of the MAEF remain to be explored. This study employs finite element analysis (FEA) to compare the biomechanical characteristics of PSISF and evaluate the biomechanical properties of MAEF for treating TTBFs, thereby providing a biomechanical foundation for MAEF's clinical application.

2. Materials and Methods

2.1. Finite Element Model of the Adult

Establishment and Validation of the T11-L3 Thoracolumbar Finite Element Model DICOM files for finite element modeling (T11-L3 thoracolumbar spine) were acquired from a healthy volunteer (30-year-old male, weight 76 kg, height 178 cm) using 64-slice spiral CT. A three-dimensional (3D) contour model of T11-L3 was extracted using Mimics 20.0 (Materialise, Belgium) software through threshold segmentation, dynamic growth, mask editing, and Boolean operations. Using Geomagic 2012 (Geomagic, USA), slices of the contour model were captured, followed by smoothing, polishing, denoising, surface construction, and solidification. The model then entered the polygon processing stage, underwent surface patch distribution, and finally underwent surface solidification encapsulation to generate a 3D IGES file format (Fig. 1A).

SolidWorks 2015 (Dassault Systèmes, France) was used to reconstruct the intervertebral disc (matrix and nucleus pulposus) and articular surfaces. The reconstructed vertebral body comprised cortical bone, cancellous bone, and endplates. The intervertebral disc consisted of nucleus pulposus and annulus fibrosus (4:6 ratio). the thickness of the cortical bone was set to 1 mm, and the endplate was set to 0.5 mm, with friction contact occurring between superior and inferior articular cartilages at a coefficient of 0.1[15]. Seven accessory ligaments were added, including the anterior longitudinal ligament, posterior longitudinal ligament, ligamentum flavum, interspinous ligaments, supraspinous ligament, capsular ligament, and intertransverse ligaments, resulting in the final normal model (Fig. 1B).

2.2. Establishment of Fracture Models and Fixation Systems

To establish a thoracolumbar fracture model, vertebral resection (laminectomy) was employed to simulate vertebral fracture. Specifically, half of the L1 vertebral cancellous bone was removed to reduce anterior vertebral support strength; the posterior structure was preserved to create a finite element model of an unstable thoracolumbar fracture[16] (Fig. 1C). The dimensions of the internal fixation devices used are as follows: all screws have a diameter of 5.0 mm, and all connecting rods have a diameter of 5.5 mm, three-dimensional solid modeling was performed using SolidWorks 2015 (Dassault Systèmes, France) to complete the modeling and assembly of the implant components (Figs. 1D and 1E).

The assembled solid model was imported into Ansys Workbench 18.0 (Ansys, USA) for Boolean operations. Material parameters (Table 1) were assigned[16, 17], contacts were defined, and free mesh generation was performed using Solid 186 solid elements (Table 2). Ligament Modeling Based on the established model, ligament attachment points were identified according to physiological characteristics. Link180 elements were used for meshing, with the property set to stretchable but not compressible.

Contact settings between components are configured based on actual conditions: smooth frictionless contact between small joints, rigid contact between nails and bones, and rigid contact between nail heads and joints. The friction coefficient for the intermediate rotating pair in the MAEF model is set to 0.05. The rear spring-like support device is designed for compression only, with spring compression force controlled within the range of 17–350 N.

2.3. Finite Element Simulation

The lower surface of the L3 vertebral body is fixedly constrained. A 400N preload and a pure bending moment of 7.5Nm are applied to the T11 vertebral body. The percentage change in ROM before and after fixation, the maximum stress values at the fixation system, the fractured vertebral body (L1), the inferior endplate of T12, and the superior endplate of L2 are recorded for both models.

3. Results

3.1. Validation of the Complete Model (T11-L3)

To evaluate the validity of the intact T11-L3 model, a 7.5 Nm torque was applied to simulate physiological loading forces. Under conditions of flexion, extension, lateral flexion left, lateral flexion right, rotation left, and rotation right, the ROM of the T11-L3 intact spinal model was 5.92°, 6.41°, 7.92°, 7.64°, 3.43°, and 3.95°, respectively. These values are comparable to previously reported experimental data[16, 18, 19], thereby validating the model's reasonableness.

3.2. Range of Motion (ROM)

Under six working conditions—flexion, extension, left lateral flexion, right lateral flexion, left rotation, and right rotation—the ROM values for the normal model (T11-L3) are 5.92°, 6.41°, 7.92°, 7.64°, 3.43°, and 3.95°, respectively; The normal model (T12-L2) exhibited ROM values of 3.77°, 3.68°, 4.38°, 4.24°, 2.23°, and 2.32°; The ROM values for the MAEF model were 0.92°, 0.85°, 1.04°, 1.05°, 0.32°, and 0.33°; The ROM values for the PSISF model were 3.53°, 5.36°, 4.29°, 4.41°, 2.22°, and 2.77°. The ROM of the MAEF model was 8.4%–15.5% of the normal lumbar spine model (T11–L3), while the ROM of the PSISF model was 48.0%–70.9% of the normal lumbar spine model (T12–L2). Thus, both fixed models restricted the ROM of the normal model, with the MAEF model exhibiting more pronounced restriction (Fig. 2).

3.3. Von Mises Stress of Fixation Systems

Under all loading conditions, the maximum stress values in the MAEF model fixation system were lower than those in the PSISF model fixation system. The maximum stresses for both models occurred during left and right rotation. The MAEF model fixation system reached its maximum stress of 77.025 MPa during right rotation, while the PSISF model fixation system peaked at 170.97 MPa during left rotation. Stress distribution plots reveal that the MAEF model exhibits more dispersed stresses across all operating conditions, whereas the PSISF model shows significantly more concentrated stresses, particularly during left and right rotation. The maximum stress values and stress distribution plots for both models under six operating conditions (Fig. 3).

3.4. Maximum stress values at the fractured vertebral body (L1) and adjacent endplates.

Under all loading conditions, the maximum stress values in the fractured vertebral body (L1) of the PSISF model exceeded those of the MAEF model (Fig. 4A). Specifically, the PSISF model exhibited 1.42 times higher stress during flexion, 1.23 times higher during extension, 10.62 times higher during left lateral flexion, 8.63 times higher during right lateral flexion, 5.27 times higher during left rotation, and 3.64 times higher during right rotation.

Under all loading conditions, the maximum stress values at the inferior endplate of T12 in the PSISF model exceeded those in the MAEF model (Fig. 4B). Specifically, the PSISF model exhibited 2.03 times higher stress during flexion, 4.17 times higher during extension, 3.83 times higher during left flexion, 6.58 times higher during right flexion, 1.36 times higher during left rotation, and 1.43 times higher during right

rotation. The maximum stress values at the L2 superior endplate in the PSISF model were consistently higher than those in the MAEF model (Fig. 4C), specifically: 4.30 times higher during flexion, 4.96 times higher during extension, 2.90 times higher during left flexion, 3.14 times higher during right flexion, 2.22 times higher during left rotation, and 1.43 times higher during right rotation. Figure 4D displays the contour plots of the T12 inferior endplate, fractured vertebral body (L1), and L2 superior endplate under six loading conditions.

4. Discussion

The optimal surgical approach for TTBFs remains highly controversial among spinal surgeons[20–22]. Compared to traditional open posterior surgery, minimally invasive pedicle screw fixation offers advantages such as shorter operative time, reduced trauma, and faster recovery, leading to increasing recommendations by scholars[23–25]. However, even with the addition of two screws to the PSISF at the fracture plane, biomechanical deficiencies persist, potentially leading to internal fixation failure and progressive kyphosis worsening[7, 26]. As documented in the literature[27, 28], numerous modified approaches exist, such as transpedicular vertebral body reinforcement or combined anterior-posterior procedures, aimed at reducing complications; yet outcomes remain controversial.

MAEF offers a potential solution to this problem. Using a minimally invasive approach, four pedicle screws are placed bilaterally on either side of the injured vertebra. MAEF provides enhanced fixation strength, and its adjustable modular design allows further correction for potential loss of reduction. Furthermore, after callus formation at the fracture site, localized micro-movement stimulates callus formation, preventing progressive spinal kyphosis. This technique operates on principles similar to the accordion bone grafting technique[29, 30] .

As observed in our study, the MAEF model exhibited ROM ranging from 8.4% to 15.5% of a normal lumbar spine model (T11-L3), while the PSISF model demonstrated ROM between 48.0% and 70.9% of a normal lumbar spine model (T12-L2). The MAEF model significantly restricts lumbar ROM compared to the PSISF model, providing superior stability conditions for healing thoracolumbar burst fractures.

It is well-known that axial rotational motion warrants attention. Cadaver biomechanical studies indicate that compared to intact spines, internal fixation systems exhibit significantly reduced stiffness during axial rotation, making them more susceptible to failure and fracture[31, 32]. This study also observed that the MAEF model exhibited lower maximum stress values in all loading conditions, particularly during lateral rotation. This indicates superior protection against axial rotation in the MAEF model, reducing the likelihood of fracture failure under equivalent loading conditions. Stress contour plots also reveal significantly higher and more concentrated stresses in the PSISF model across all loading conditions. This contrasts with the MAEF model, which features a longer fixation segment and a posterior micro-adjustable expansion device that distributes stresses throughout the entire fixation system.

This study reveals a significant finding that may explain the favorable outcomes observed in patients treated with the MAEF model in the previous study[14]. We observed that although the MAEF model involves long-segment fixation, the maximum stress values at the fractured vertebral body (L1) under flexion and extension conditions are comparable to those of the PSISF model. However, the maximum stress values at the fractured vertebral body (L1) under four conditions—left flexion, right flexion, left rotation, and right rotation—are significantly lower than those of the PSISF model. Under all loading conditions, the MAEF model exhibited the lowest maximum stress values at the adjacent vertebral endplates during flexion and extension. This indicates that the MAEF model provides superior stability to the fractured vertebra under left flexion, right flexion, left rotation, and right rotation conditions. Under flexion and extension conditions, the micro-adjustable system permits axial stress to act on the fractured vertebra, avoiding stress shielding caused by long-segment fixation and promoting fracture healing[33–35] .

Our study has limitations. Finite element analysis can only simulate spinal motion in six directions, potentially failing to fully replicate all human characteristics. Although both models are minimally invasive fixation systems, the MAEF model employs long-segment fixation, offering more pronounced mechanical advantages. We plan to supplement future work with finite element testing comparing it to traditional open long-segment fixation. The posterior micro-adjustable system cannot fully represent actual mechanical conditions within finite element components.

5. Conclusion

The novel external fixation device offers superior stress distribution compared to traditional percutaneous short-segment interbody screw fixation, providing enhanced stability while avoiding secondary surgical trauma. Its micro-adjustable system permits mechanical stimulation of fractured vertebral bodies under flexion conditions, preventing stress shielding. Furthermore, it has demonstrated satisfactory clinical outcomes in early applications.

Declarations

Data availability statement

Data are available from the corresponding author upon request.

Consent for publication

Not applicable to this manuscript.

Ethics Statement and consent to participate

The study was approved by the Ethics Committee of the PLA General Hospital (S2020–114-01). This study complies with the Declaration of Helsinki. Written informed consent was obtained from all

individual participants included in the study.

Conflicts of Interest

Each author certifies that he has no commercial associations that might pose a conflict of interest with the submitted article.

Authors' Contributions

Shaobo Nie did the conception and design. Hui Guo and Jiahao Feng performed the acquisition of data. Yanyan Xue and Hui Guo performed the analysis and interpretation of data. Shaobo Nie, Ming Hao and Kun Wang critically revised the article. All authors reviewed the submitted version of the manuscript. Shaobo Nie approved the final version of the manuscript on behalf of all authors. Shaobo Nie, Ming Hao, and Kun Wang supervised the study. Hui Guo, Jiahao Feng, and Yanyan Xue contributed equally to this work.

Funding

The authors declare that this study received no funding.

References

1. Smits, A.J., et al., *Incidence of Traumatic Spinal Fractures in the Netherlands: Analysis of a Nationwide Database.* Spine, 2020. **45**(23): p. 1639-1648.
2. Zileli, M., S. Sharif, and M. Fornari, *Incidence and Epidemiology of Thoracolumbar Spine Fractures: WFNS Spine Committee Recommendations.* Neurospine, 2021. **18**(4): p. 704-712.
3. Lang, S., et al., *Increased incidence of vertebral fractures in German adults from 2009 to 2019 and the analysis of secondary diagnoses, treatment, costs, and in-hospital mortality.* Sci Rep, 2023. **13**(1): p. 6984.
4. Han, Y., et al., *Percutaneous monoplanar screws versus hybrid fixed axial and polyaxial screws in intermediate screw fixation for traumatic thoracolumbar burst fractures: a case-control study.* J Orthop Surg Res, 2024. **19**(1): p. 85.
5. Alimohammadi, E., et al., *Analysis of factors associated with the failure of treatment in thoracolumbar burst fractures treated with short-segment posterior spinal fixation.* J Orthop Surg Res, 2023. **18**(1): p. 690.
6. Verlaan, J.J., et al., *Clinical and radiological results 6 years after treatment of traumatic thoracolumbar burst fractures with pedicle screw instrumentation and balloon assisted endplate reduction.* Spine J, 2015. **15**(6): p. 1172-8.
7. Lainé, G., et al., *Risk factors for kyphosis recurrence after implant removal in percutaneous osteosynthesis for post-traumatic thoracolumbar fracture.* Eur Spine J, 2024. **33**(4): p. 1597-1606.

8. Chen, C., et al., *Posterior short-segment instrumentation and limited segmental decompression supplemented with vertebroplasty with calcium sulphate and intermediate screws for thoracolumbar burst fractures.* Eur Spine J, 2014. **23**(7): p. 1548-57.
9. Moura, D.L., *The role of kyphoplasty and expandable intravertebral implants in the acute treatment of traumatic thoracolumbar vertebral compression fractures: a systematic review.* EFORT Open Rev, 2024. **9**(4): p. 309-322.
10. Chen, C., et al., *Single-Stage Posterior Unilateral Transpedicular Corpectomy With Circumferential Reconstructive Stabilization for the Treatment of Severe Thoracic and Lumbar Complete Burst Fractures.* Global Spine J, 2025: p. 21925682251338789.
11. Shen, H.Q., et al., *Treatment of thoracolumbar fractures with severe collapse of the anterior and middle columns via balloon-assisted endplate reduction, transpedicular bone grafting and pedicle screw fixation.* J Orthop Surg Res, 2025. **20**(1): p. 580.
12. Ge, T., et al., *Impact of traumatic intervertebral disc injury on loss of correction following pedicle screw fixation for thoracolumbar fractures.* BMC Musculoskelet Disord, 2025. **26**(1): p. 507.
13. Aono, H., et al., *Surgical outcomes of temporary short-segment instrumentation without augmentation for thoracolumbar burst fractures.* Injury, 2016. **47**(6): p. 1337-44.
14. Nie, S., et al., *Pedicle screw fixation with a novel external frame for thoracolumbar fractures: A comparative study.* Journal of Orthopaedic Translation, 2020. **25**: p. 60-65.
15. Chosa, E., et al., *Analysis of the effect of lumbar spine fusion on the superior adjacent intervertebral disk in the presence of disk degeneration, using the three-dimensional finite element method.* J Spinal Disord Tech, 2004. **17**(2): p. 134-9.
16. Liao, J.C., W.P. Chen, and H. Wang, *Treatment of thoracolumbar burst fractures by short-segment pedicle screw fixation using a combination of two additional pedicle screws and vertebroplasty at the level of the fracture: a finite element analysis.* BMC Musculoskelet Disord, 2017. **18**(1): p. 262.
17. Basaran, R., et al., *Finite Element Analysis of Short- Versus Long-Segment Posterior Fixation for Thoracolumbar Burst Fracture.* World Neurosurg, 2019. **128**: p. e1109-e1117.
18. Xilong, C., et al., *Biomechanical Comparison of Different Treatment Strategies for Thoracolumbar Burst Fracture: A Finite Element Study.* World Neurosurg, 2023. **180**: p. e429-e439.
19. Cardenas, R.J., et al., *Comparison of allograft bone and titanium cages for vertebral body replacement in the thoracolumbar spine: a biomechanical study.* Neurosurgery, 2010. **66**(6 Suppl Operative): p. 314-8; discussion 318.
20. Trungu, S., et al., *Percutaneous pedicle screw fixation without arthrodesis of 368 thoracolumbar fractures: long-term clinical and radiological outcomes in a single institution.* Eur Spine J, 2023. **32**(1): p. 75-83.
21. Hong, S.H., et al., *Minimally Invasive Spine Surgery versus Open Posterior Instrumentation Surgery for Unstable Thoracolumbar Burst Fracture.* Asian Spine J, 2021. **15**(6): p. 761-768.
22. Greiner-Perth, A.K., H.J. Wilke, and C. Liebsch, *Which spinal fixation technique achieves which degree of stability after thoracolumbar trauma? A systematic quantitative review.* Spine J, 2025. **25**(3): p. 515-

567.
23. Esposito, F., et al., *Outcome Measures of Open versus Minimally Invasive Surgery for Thoracolumbar Spinal Traumatic Fractures: A Systematic Review and Meta-Analysis.* J Clin Med, 2024. **13**(18).
24. Daher, M., et al., *Minimally Invasive Versus Open Surgery for Thoracolumbar Fractures Treatment : A Meta-analysis of Randomized Controlled Trials and Prospective Studies.* Spine (Phila Pa 1976), 2025. **50**(6): p. 412-419.
25. Sebaaly, A., et al., *Percutaneous fixation of thoracolumbar vertebral fractures.* EFORT Open Rev, 2018. **3**(11): p. 604-613.
26. Kanna, R.M., A.P. Shetty, and S. Rajasekaran, *Posterior fixation including the fractured vertebra for severe unstable thoracolumbar fractures.* Spine J, 2015. **15**(2): p. 256-64.
27. Aono, H., et al., *Temporary short-segment pedicle screw fixation for thoracolumbar burst fractures: comparative study with or without vertebroplasty.* Spine J, 2017. **17**(8): p. 1113-1119.
28. Guo, H., et al., *A Finite Element Study on the Treatment of Thoracolumbar Fracture with a New Spinal Fixation System.* Biomed Res Int, 2021. **2021**: p. 8872514.
29. Wang, D., et al., *Evaluating Docking Site Local Hematoma Formation and Blood Flow on its Healing Using the Accordion Technique at the End of Tibial Bone Transport.* Orthop Surg, 2024. **16**(9): p. 2264-2272.
30. Gulabi, D., et al., *Ilizarov fixator combined with an intramedullary nail for tibial nonunions with bone loss: is it effective?* Clin Orthop Relat Res, 2014. **472**(12): p. 3892-901.
31. Panchal, R.R., et al., *Is lateral stabilization enough in thoracolumbar burst fracture reconstruction? A biomechanical investigation.* Spine J, 2015. **15**(10): p. 2247-53.
32. Bishop, F.S., et al., *The biomechanical contribution of varying posterior constructs following anterior thoracolumbar corpectomy and reconstruction.* J Neurosurg Spine, 2010. **13**(2): p. 234-9.
33. Gupta, R.R., et al., *Axial strain enhances osteotomy repair with a concomitant increase in connexin43 expression.* Bone Res, 2015. **3**: p. 15007.
34. Chao, E.Y., et al., *Enhancement of fracture healing by mechanical and surgical intervention.* Clin Orthop Relat Res, 1998(355 Suppl): p. S163-78.
35. Wu, W., et al., *Biomechanical Effects of Mechanical Stress on Cells Involved in Fracture Healing.* Orthop Surg, 2024. **16**(4): p. 811-820.

Tables

Tables 1 and 2 are available in the supplementary files section

Figures

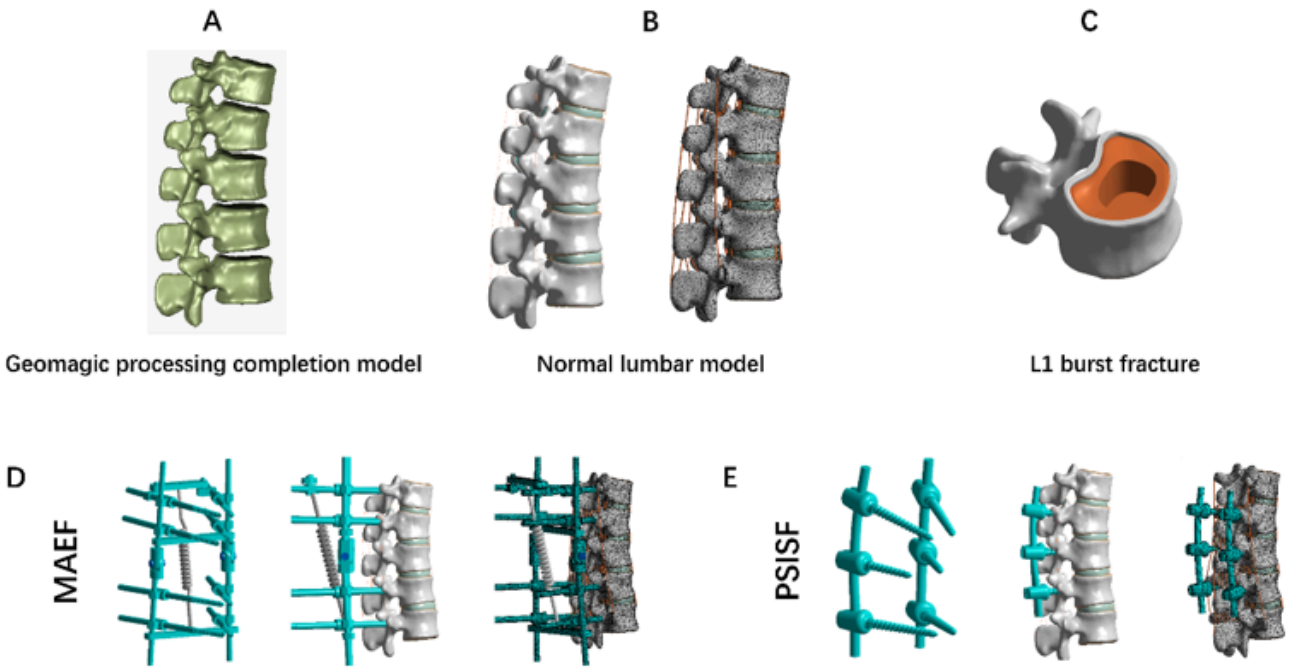


Figure 1

(A) Geomagic processing completion model. (B) Normal lumbar model. (C) L1 burst fracture. (D) MAEF model. (E) PSISF model.

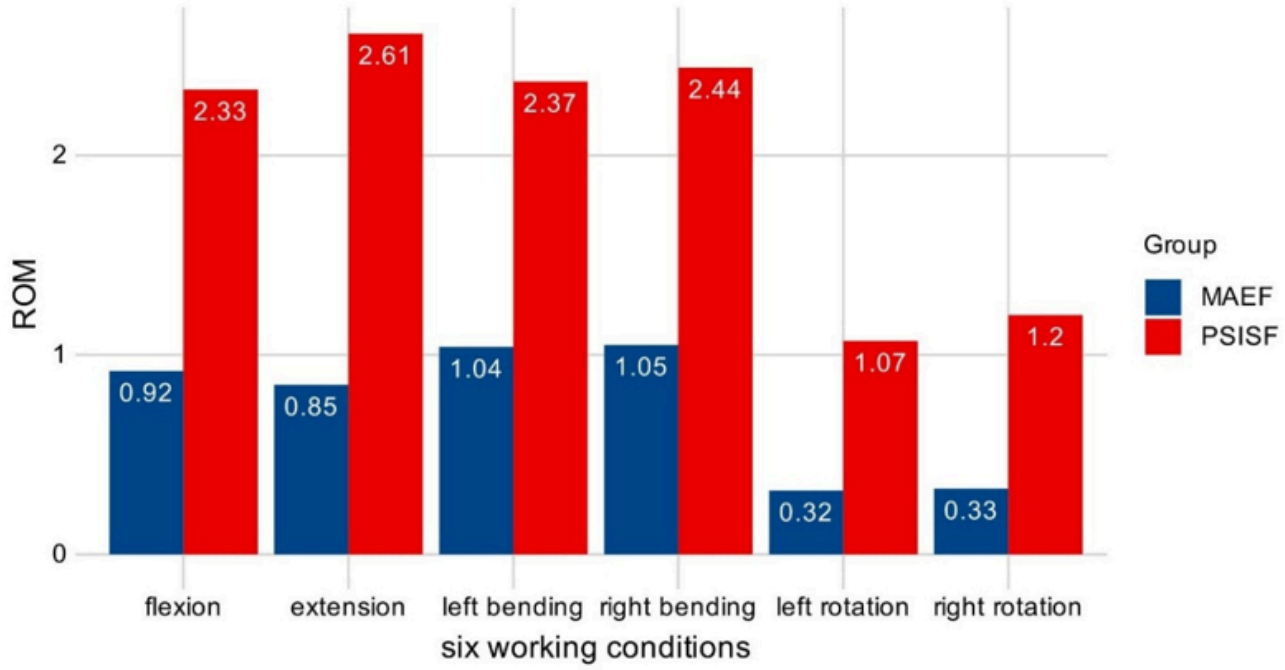
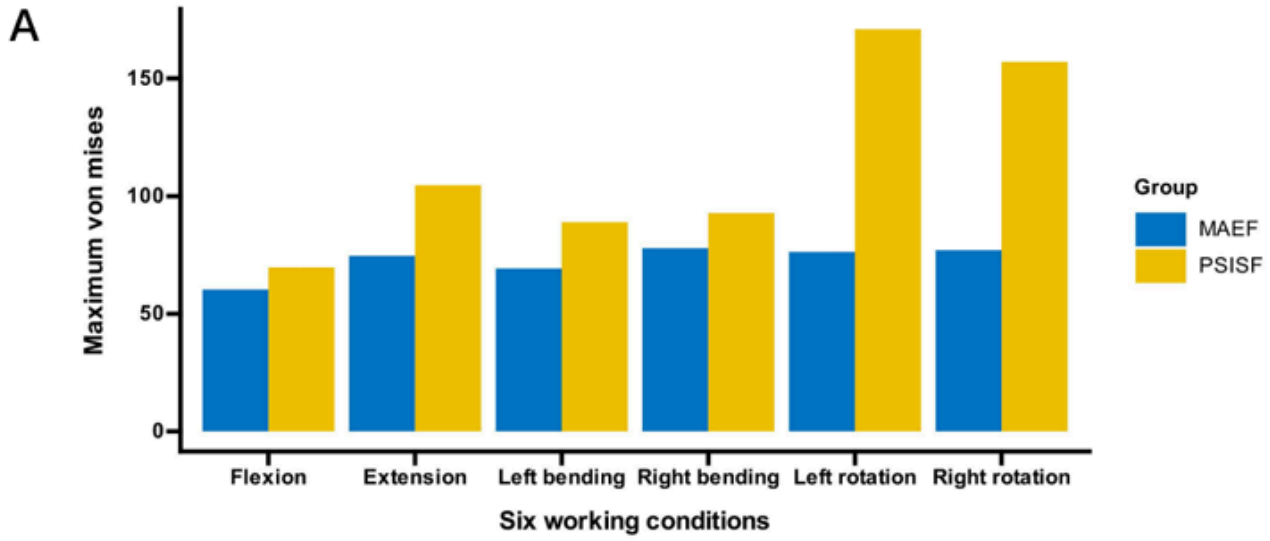


Figure 2

Range of Motion (ROM).



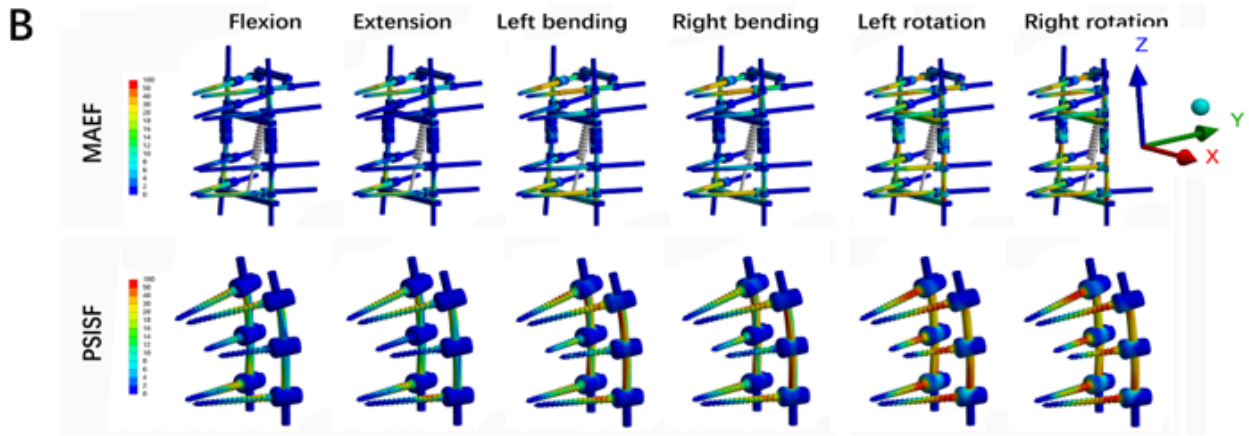


Figure 3

The maximum stress values and stress distribution plots for both models under six operating conditions.

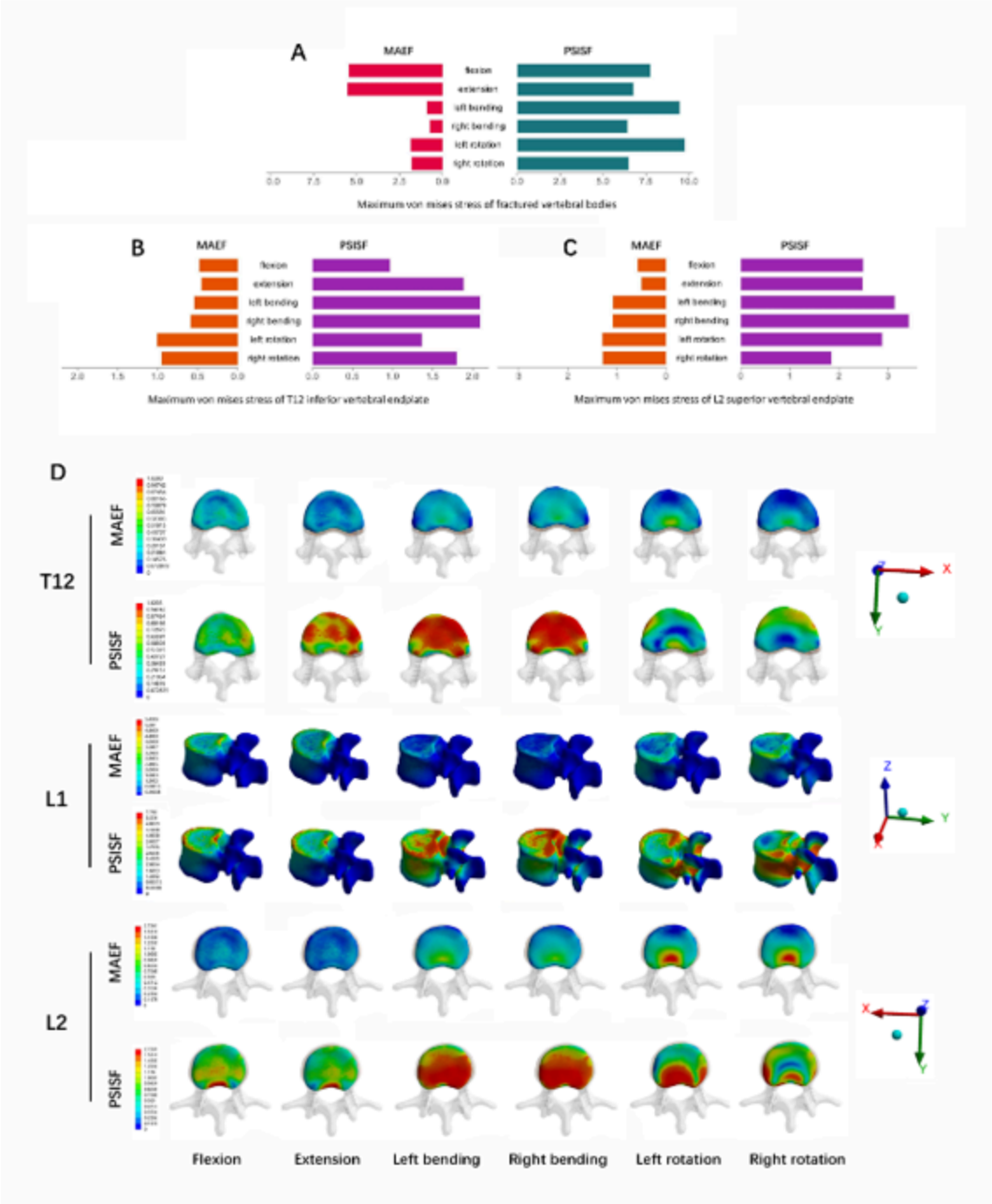


Figure 4

(A) Under all loading conditions, the maximum stress values in the fractured vertebral body (L1) of the PSISF model exceeded those of the MAEF model. (B) Under all loading conditions, the maximum stress values at the inferior endplate of T12 in the PSISF model exceeded those in the MAEF model. (C) The maximum stress values at the L2 superior endplate in the PSISF model were consistently higher than those in the MAEF model.

Supplementary Files

This is a list of supplementary files associated with this preprint. Click to download.

- Table2StatisticsonElementandNodeCounts1.jpg
- Table1MaterialParameters1.jpg